INSTITUTE OF PHYSICS PUBLISHING JOURNAL OF OPTICS B: QUANTUM AND SEMICLASSICAL OPTICS
J. Opt. B: Quantum Semiclass. Opt. **7** (2005) 253–263 doi:10.1088/1464-4266/7/9/004

Coupled mode competition in unstable resonators using the exact cavity equations of motion with dynamic gain

Manuel Guizar-Sicairos and Julio C Gutiérrez-Vega[1]

Photonics and Mathematical Optics Group, Tecnológico de Monterrey, Monterrey 64849, Mexico

E-mail: juliocesar@itesm.mx

Received 22 February 2005, accepted for publication 19 May 2005
Published 2 August 2005
Online at stacks.iop.org/JOptB/7/253

Abstract
The dynamic coupled mode (DCM) method has been applied to study the transverse mode competition in optical resonators. In this work a differential equation for the homogeneously saturating dynamic gain is included in the original dynamic coupled mode method, thus increasing its physical resemblance and allowing the retrieval of gain temporal evolution at every point within the lasing medium. This new model provides a realistic temporal evolution of the mode competition and gain saturation within the resonator, which can give further information on spatial coherence properties. The new general formulation does not assume that lasing medium fills the optical cavity and is suitable for modelling the dependence of small-signal gain and power gain on the transverse and longitudinal coordinates. The application of the method to a typical CO_2 unstable confocal resonator is fully described; results and their connection to relevant physical properties of gas lasers, such as spiking and relaxation oscillations, are discussed. Results of the numerical implementation of the DCM method with dynamic gain are in very good agreement with experimental measurements reported previously.

Keywords: dynamic coupled modes, mode competition, dynamic gain equation

1. Introduction

There are hardly a handful of ways to address the problem of estimating the laser output, including the effects of homogeneously saturating gain, for an arbitrary mirror geometry. The traditional approach to compute the effects of saturable gain in a standing or ring optical resonant cavity is to place a finite number of gain sheets along the optical cavity and propagate a single wavefront in a manner pioneered by Fox and Li [1] until the wavefront is unchanged after a round trip propagation.

Though this method is extremely useful to estimate the mode volume and steady state field structure within the cavity, it is not possible to extract any temporal evolution information from this approach, and there is no direct expression to relate the results to the bare cavity modes, nor to their well studied spatial coherence properties. Furthermore, this method implicitly assumes that the gain changes slowly enough to be considered quasi-static over the time interval covered by a round trip propagation, and is inappropriate for pulsed lasers where a steady state of both the gain and the optical field may not occur.

The diffractive mode structure properties of optical resonators were first analysed by Fox and Li with the publication of their well known paper on the resonant modes in a maser interferometer [2]. Later in 1980, Siegman developed a theoretical framework to compute the exact cavity equations of motion for an arbitrary resonator [3], using for the first time an expansion of the cavity field in a basis set directly related to the transverse eigenmodes of the bare cavity, thus including an

[1] Author to whom any correspondence should be addressed.

arbitrary amount of diffraction loss or output coupling at one end.

The inclusion of the diffractive losses in the unstable cavity model is crucial, but it also complicates obtaining useful information from exclusively analytical models, and consequently numerical simulations of optical cavities became necessary. However, most of the analysis of unstable resonators has centred on the optical properties of the bare cavity and gain effects have been considered only to derive a modified fundamental field distribution and the spatially varying, but time independent, gain saturation [4].

In 1990 Bowers and Moody outlined a numerical procedure to compute the time dependent three-dimensional field in unstable resonators [5]. The dynamic coupled mode (DCM) method expands the loaded cavity field into the bare cavity eigenmodes described by Siegman [6] and obtains the mode competition in a CO_2 unstable laser. Although a great deal of information of the laser steady state can be obtained with this approach, the temporal evolution of the system was of secondary interest and a simple mathematical model was used for the gain temporal dependence. The implementation of a non-dynamic gain equation forbids the retrieval of accurate temporal laser dynamics and restricts the DCM method to a steady state modal decomposition.

In this paper we incorporate a differential equation of the power gain into the DCM model. The resulting numerical method is capable of obtaining the coupled mode competition in optical cavities, and provides the complete build-up of the field within the resonator, giving a more realistic spatial and temporal evolution of the gain and further insight into the physics of unstable lasers. Although this formulation can be applied to both stable and unstable resonators, the latter require less bare cavity modes for proper convergence due to their high mode discrimination.

In order to test this novel formulation and ensure that it is accurately modelling matter–light interaction within the cavity, we numerically apply it to a typical confocal CO_2 unstable resonator to analyse its turn-on stage. This well studied example allows us to compare retrieved features of laser performance and compare them to well assessed numerical methods and analytical approximations.

Unlike most analytical approximations the presented formulation is quite general; it does not assume that the gain medium uniformly fills the resonant cavity and can account for an arbitrary transverse or longitudinal dependence of small-signal gain and saturation intensity, thus accurately modelling an arbitrary configuration.

To compare the results with typically used methods that are known to accurately retrieve some laser output features, we use a constant pump in the numerical implementation; however, the presented formulation can account for a time varying pump through temporal variation of the small-signal gain, allowing us to model pulsed or gain-switched laser systems with complete retrieval of spatio-temporal information. Furthermore, the new dynamic gain equation can be straightforwardly modified to include transverse hole burning or inhomogeneous line broadening effects.

Although we focus this work on accurate modelling of CO_2 through the dynamic gain equation, other lasing media, such as solid-state or organic dye lasers, can be modelled with the presented formalism through careful selection of parameters and proper temporal and spatial dependence of small-signal gain. Our work extends and consolidates previous studies on temporal behaviour of optical resonators [3, 5, 7–13].

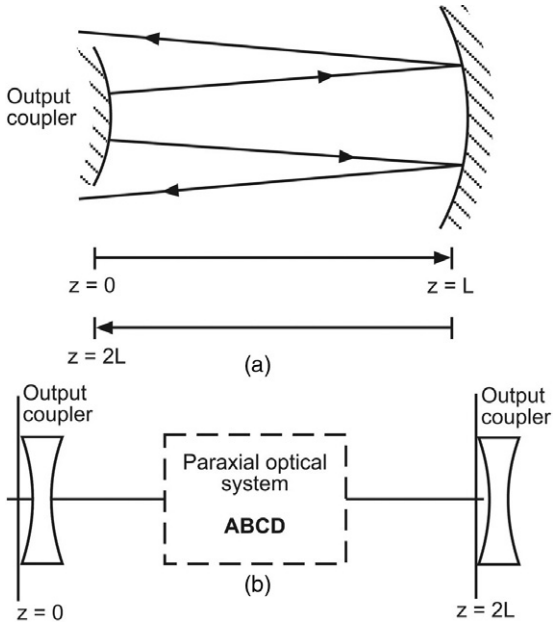

Figure 1. (a) Standing wave unstable resonator cavity. (b) Resonator lens equivalent system with single diffractive aperture. The reference plane is located just before incidence with the output coupler.

2. Exact cavity equations of motion

For completeness and to establish useful notation we will briefly describe the derivation of the exact cavity equations of motion and the simplifications that lead to the DCM method.

The derivation of the DCM method follows the analysis previously reported by Siegman [3] to retrieve the complete spatial and temporal evolution of the field inside the cavity by solving several differential equations for the modal coefficients [5].

Although the DCM model describes either a ring or standing wave laser cavity, we focus on the latter. The resonant cavity, as shown in figure 1(a), has a z axis running from $z = 0$ to L in one direction along the cavity and then from $z = L$ to $2L$ going back to the output coupler. The typical resonator lens equivalent system is depicted in figure 1(b). We will further assume that all the coupling and diffraction losses are concentrated in an output mirror located at $z = 0 = 2L$, that has an arbitrary complex amplitude reflectivity $\rho(\mathbf{r})$, where $\mathbf{r}$ is the set of transverse coordinates perpendicular to the z axis. Other intracavity components, including the primary mirror, are assumed to be loss-less; this approximation is reasonable since the diffraction losses on the primary mirror are often very small due to large mirror radius and reflectivity.

2.1. Scalar wave equation

The full vector wave equation for the optical cavity electrical field is given by [3]

$$\left(\nabla^2 - \mu_0\sigma\frac{\partial}{\partial t} - \mu_0\varepsilon\frac{\partial^2}{\partial t^2}\right)\mathbf{E}\,(\mathbf{r}, z, t) = \mu_0\frac{\partial^2\mathbf{P}\,(\mathbf{r}, z, t)}{\partial t^2}, \tag{1}$$

where $\mathbf{E}(\mathbf{r}, z, t)$ is the electrical field inside the cavity, $\mathbf{P}(\mathbf{r}, z, t)$ is the polarization which accounts for effects of laser atomic transitions, including spontaneous emission [5], μ_0 is the magnetic permeability of free space, ε is the electrical permittivity in the cavity and σ is the conductivity of the medium accounting for a linear distribution of the losses inside the resonator.

Assuming that $\mathbf{E}(\mathbf{r}, z, t)$ and $\mathbf{P}(\mathbf{r}, z, t)$ have slow varying amplitudes and phases referenced to the carrier frequency ω_0, even if not compared to a single round trip, and are propagating in the positive z-direction, both $\mathbf{E}$ and $\mathbf{P}$ may be converted to complex phasor amplitudes

$$\mathbf{E}\,(\mathbf{r}, z, t) = \mathrm{Re}\{\tilde{\mathbf{E}}\,(\mathbf{r}, z, t)\exp[\mathrm{i}\,(\omega_0 t - k_0 z)]\}, \tag{2}$$

$$\mathbf{P}\,(\mathbf{r}, z, t) = \mathrm{Re}\{\tilde{\mathbf{P}}\,(\mathbf{r}, z, t)\exp[\mathrm{i}\,(\omega_0 t - k_0 z)]\}, \tag{3}$$

where $k_0 = \omega_0(\mu_0\varepsilon)^{1/2}$. The carrier frequency ω_0 is arbitrary but is conveniently defined as $2\omega_0 L/c = 2\pi q_0$, where q_0 is any axial-mode integer near the line centre and $c = 1/(\mu_0\varepsilon)^{1/2}$. Applying the paraxial and slow envelope approximation, expression (1) becomes

$$\left[\nabla_\mathrm{t}^2 - 2\mathrm{i}k_0\left(\frac{\partial}{\partial z} + \frac{\alpha_0}{c} + \frac{1}{c}\frac{\partial}{\partial t}\right)\right]\tilde{\mathbf{E}}\,(\mathbf{r}, z, t) = -\omega_0^2\mu_0\tilde{\mathbf{P}}\,(\mathbf{r}, z, t)\,, \tag{4}$$

where $\alpha_0 \equiv \sigma/2\varepsilon$, and ∇_t^2 is the transverse Laplacian.

Let us assume that the response of the lasing medium to the electric field is collinear; in this approximation the polarization is

$$\tilde{\mathbf{P}}\,(\mathbf{r}, z, t) = \mathrm{i}\frac{\varepsilon}{k_0}g\,(\mathbf{r}, z, t)\,\tilde{\mathbf{E}}\,(\mathbf{r}, z, t) \tag{5}$$

for frequencies near the line centre, where $g(\mathbf{r}, z, t)$ is the power gain coefficient. We will further assume that there are no polarizing or anisotropic elements within the cavity, thus the polarization is preserved and vector notation may be dropped [4],

$$\left[\nabla_\mathrm{t}^2 - 2\mathrm{i}k_0\left(\frac{\partial}{\partial z} + \frac{\alpha_0}{c} - \frac{1}{2}g\,(\mathbf{r}, z, t) + \frac{1}{c}\frac{\partial}{\partial t}\right)\right] \times \tilde{E}\,(\mathbf{r}, z, t) = 0, \tag{6}$$

with

$$\tilde{E}\left(\mathbf{r}, z = 0^+, t\right) = \rho(\mathbf{r})\tilde{E}\left(\mathbf{r}, z = 2L^-, t\right) \tag{7}$$

the boundary condition for the complex field amplitude due to reflection at the output mirror, where L is the length of the standing wave cavity; $z = 0^+$ indicates that the field is just leaving the reference plane, whereas $z = 2L^-$ denotes the field amplitude just incident upon that plane.

2.2. Bare cavity modes

A note on the properties of the bare cavity lossy eigenmodes is in order. The exact, lossy stationary transverse eigenmodes of a laser cavity are solutions of the paraxial Helmholtz wave equation

$$\left[\nabla_\mathrm{t}^2 - 2\mathrm{i}k_0\frac{\partial}{\partial z}\right]u_{nm}\,(\mathbf{r}, z) = 0, \tag{8}$$

and satisfy the reduced boundary condition

$$\rho\,(\mathbf{r})\,u_{nm}\left(\mathbf{r}, 2L^-\right) = \gamma_{nm}u_{nm}\left(\mathbf{r}, 0^+\right), \tag{9}$$

at the output mirror, where γ_{nm} is the eigenvalue associated with the nmth mode.

These eigenmodes are typically computed at the output coupler feedback plane, just before reflection; in this case equations (8) and (9) can be transformed into the linear homogenous Fredholm integral equation [4]

$$\gamma_{nm}u\left(\mathbf{r}, z = 2L^-\right) = \int\rho\left(\mathbf{r}'\right)K\left(\mathbf{r}, \mathbf{r}'\right)u\left(\mathbf{r}', z = 2L^-\right)\mathrm{d}\mathbf{r}'; \tag{10}$$

in the Fresnel approximation the Huygens kernel $K(\mathbf{r}, \mathbf{r}')$ is given in terms of the cavity $ABCD$ matrix elements. The $ABCD$ matrix accounts for loss-less cavity elements excluding the output coupler. The kernel may be expressed as

$$K\left(\mathbf{r}, \mathbf{r}'\right) = \frac{\mathrm{i}k_0}{2\pi B}\exp\left\{-\frac{\mathrm{i}k_0}{2B}\left[A\left(x'^2 + y'^2\right) - 2\left(xx' + yy'\right) + D\left(x^2 + y^2\right)\right]\right\}, \tag{11}$$

when the paraxial system is azimuthally symmetric.

Due to the nature of the boundary conditions, the propagation kernel in equation (10) is not in general a Hermitian operator, hence the eigenvalues γ_{nm} will be complex and the eigenmodes will not be orthogonal in the usual sense. There will exist, however, an adjoint set of eigenfunctions $u_{nm}^\dagger(\mathbf{r}, z)$ with identical eigenvalues γ_{nm} which form a biorthonormal set to the $u_{nm}(\mathbf{r}, z)$, that is

$$\int u_{nm}(\mathbf{r}, z)u_{n'm'}^\dagger(\mathbf{r}, z)\,\mathrm{d}\mathbf{r} = \delta_{n'n}\delta_{m'm} \tag{12}$$

as derived by Siegman for $z = 0$ [14] and later formally extended to all the resonant cavity by Wright and Firth [15]. Mathematically the adjoint set functions $u_{nm}^\dagger(\mathbf{r}, z)$ satisfy equation (10) with a transposed kernel

$$\gamma_{nm}u^\dagger\left(\mathbf{r}, z = 2L^-\right) = \rho\,(\mathbf{r})\int K\left(\mathbf{r}', \mathbf{r}\right) \times u^\dagger\left(\mathbf{r}', z = 2L^-\right)\mathrm{d}\mathbf{r}', \tag{13}$$

and physically represent the eigenmodes going in the reverse direction around the same resonator. In the case of a standing wave cavity (see figure 1(a)) $A = D$, and the operator is Hermitian if the reference plane is located in the middle of the output coupler $\rho(\mathbf{r})$ [16], thus the eigenmodes would be orthogonal in the traditional sense. A little consideration then shows that at any plane within the standing wave resonator $u_{nm}(\mathbf{r}, z)$ and $u_{nm}^\dagger(\mathbf{r}, z)$ represent the same set of transverse eigenmodes of the standing wave cavity.

2.3. Dynamic coupled modes

After outlining the main properties of the bare cavity transverse eigenmodes, we now separate the time dependence from the spatial dependence in expression (6) by expanding the electric field in terms of the diffractive stationary bare cavity modes of the resonator

$$\tilde{E}\,(\mathbf{r},z,t)=\sum_{nm}A_{nm}\,(z,t)\,E_{nm}(\mathbf{r},z), \tag{14}$$

where the functional dependence of the expansion coefficients, $A_{nm}(z,t)$, is retained to allow for temporal and spatial longitudinal build-up of the cavity field. The set of oscillation eigenmodes is defined as [3]

$$E_{nm}(\mathbf{r},z)=\gamma_{nm}u_{nm}\,(\mathbf{r},z)\exp[\ln(1/\gamma_{nm})\,z/2L]; \tag{15}$$

each of these modes represents the field that would be sustained in a steady state if the cavity were filled with uniform gain medium; each mode carries $|\gamma_{nm}|^2$ less power after a reflection on the output mirror, thus accounting for diffractive losses and output coupling. Furthermore, with the exponential factor these modes satisfy the exact output-mirror boundary condition (7) and an extended wave equation obtained by replacing $\partial/\partial z$ by $\partial/\partial z+(\ln\gamma_{nm})/2L$ in expression (8).

Defining

$$\alpha_{nm}-\mathrm{i}\beta_{nm}=\frac{c}{2L}\ln(1/\gamma_{nm})\,, \tag{16}$$

the oscillation eigenmodes may be expressed as

$$E_{nm}(\mathbf{r},z)=u_{nm}\,(\mathbf{r},z)\exp[(\alpha_{nm}-\mathrm{i}\beta_{nm})\,(z-2L)\,/c], \tag{17}$$

where α_{nm} and β_{nm} are real quantities that represent, for each transverse mode, the time decay rate and frequency offset respectively. Completeness of the set of steady-state transverse modes supported by an optical cavity has already been demonstrated by Oughstun [17].

Substituting equation (14) into (6) and using (8) and the biorthogonality relationship, we obtain the coupled differential equations for the expansion coefficients $A_{nm}(z,t)$, namely

$$\left(\frac{\partial}{\partial t}+\alpha_0+\alpha_{nm}-\mathrm{i}\beta_{nm}+c\frac{\partial}{\partial z}\right)A_{nm}\,(z,t)$$
$$=\frac{c}{2}\sum_{n'm'}\mathbf{G}_{nm,n'm'}\,(z,t)\,A_{n'm'}\,(z,t)\,, \tag{18}$$

where the elements of the array $\mathbf{G}_{nm,n'm'}(z,t)$ are given by

$$\mathbf{G}_{nm,n'm'}\,(z,t)=\exp\{[(\alpha_{n'm'}-\alpha_{nm})$$
$$-\mathrm{i}\,(\beta_{n'm'}-\beta_{nm})]\,(z-2L)\,/c\}$$
$$\times\int\mathrm{d}\mathbf{r}\;u^{\dagger}_{nm}\,(\mathbf{r},z)\,g\,(\mathbf{r},z,t)\,u_{n'm'}\,(\mathbf{r},z)\,; \tag{19}$$

in expressions (18) and (19) it is evident that the gain couples different oscillation eigenmodes.

As we stated earlier, each oscillating eigenmode satisfies the exact boundary condition (7); this means that the boundary condition on the expansion coefficients is

$$A_{nm}\,(0,t)=A_{nm}\,(2L,t)\,; \tag{20}$$

this allows the expansion of the transverse amplitude coefficients as a Fourier series of longitudinal modes:

$$A_{nm}\,(z,t)=\sum_{q}A_{nmq}\,(t)\exp(-\mathrm{i}\pi qz/L), \tag{21}$$

where each longitudinal mode is numbered with respect to the central value q_0 so that $(q+q_0)$ is the actual axial mode number; the resonance frequency of each longitudinal mode is given by

$$\omega_{nmq}=\omega_0+\frac{\pi qc}{L}+\beta_{nm}=(q+q_0)\,\frac{\pi c}{L}+\beta_{nm}. \tag{22}$$

Substituting the longitudinal expansion into (18) leads to

$$\frac{\mathrm{d}A_{nmq}(t)}{\mathrm{d}t}+\left[(\alpha_0+\alpha_{nm})-\mathrm{i}\left(\beta_{nm}+\frac{\pi qc}{L}\right)\right]A_{nmq}(t)$$
$$=\frac{c}{4L}\sum_{n'm'q'}\mathbf{G}_{nmq,n'm'q'}(t)A_{n'm'q'}(t), \tag{23}$$

with

$$\mathbf{G}_{nmq,n'm'q'}\,(t)=\int_0^{2L}\mathrm{d}z\exp[\mathrm{i}\pi z(q-q')/L]$$
$$\times\exp\{[(\alpha_{n'm'}-\alpha_{nm})-\mathrm{i}\,(\beta_{n'm'}-\beta_{nm})]\,(z-2L)\,/c\}$$
$$\times\int\mathrm{d}\mathbf{r}\;u^{\dagger}_{nm}\,(\mathbf{r},z)\,g\,(\mathbf{r},z,t)\,u_{n'm'}\,(\mathbf{r},z)\,. \tag{24}$$

The coefficients are reduced to be exclusively time dependent, hence allowing the straightforward application of standard well known numerical methods. The coupling of different transverse and longitudinal modes through the gain is explicitly seen in expressions (23) and (24).

Note that with the DCM method the complete temporal and spatial build-up of the cavity field may be retrieved by solving several coupled differential equations of first order. The intrinsic non-linear dependence of the homogeneously saturating gain $g(\mathbf{r},z,t)$ makes analytic solution of the problem difficult, thus a numerical approach is necessary.

The above formulation is quite general and applies whenever the linear susceptibility approximation is valid and the losses in the primary mirror and intracavity elements are negligible, i.e. the lasing medium and optical elements preserve the field polarization and a large feedback mirror is used. The frequency dependence of the resonant susceptibility of the lasing medium has been ignored in (5), thus the formulation applies whenever the frequency is close to the line centre and effects of frequency dependent gain are not considered. This is a good approximation when the laser curve is sufficiently broad that the transverse and longitudinal modes are affected by the 'same' gain, as is usually the case for CO_2 lasers [5]. Although the DCM model is particularly suitable for CO_2 gas systems, it can be applied anywhere the frequency dependence of the gain can be neglected.

Since most of the optical cavities have circular primary and output mirrors it is useful to apply further simplifications to the DCM method. In the appendix we review the relevant modifications to the formulation regarding axial symmetry. From this point equations from the appendix are cited in this paper.

3. Physical model for the dynamic gain

In order to retrieve laser performance and output characteristics, either numerically or by analytic approximation, authors commonly use the non-dynamic gain saturation equation [4, 5, 18–22] given by

$$g(\mathbf{r}, z) = \frac{g_0(\mathbf{r})}{1 + [I(\mathbf{r}, z) + I(\mathbf{r}, 2L - z)]/I_{\text{sat}}}, \tag{25}$$

thus forbidding accurate retrieval of temporal laser dynamics. This equation was used by Bowers and Moody [5] to exemplify the DCM numerical implementation, and restricted the results to a steady state modal decomposition of the laser output.

3.1. Differential equation for the dynamic gain $g(\mathbf{r}, z, t)$

The coupled laser rate equations for single operation mode are commonly used to model lasing behaviour with homogeneous line broadening and give an approximate dynamic of the inversion density and number of photons [11]. We have modified this formulation to include multiple-mode operation and obtain the following differential equation for the dynamic power gain $g(\mathbf{r}, z, t)$:

$$\tau \frac{\partial g(\mathbf{r}, z, t)}{\partial t} = g_0(\mathbf{r}, z, t) - g(\mathbf{r}, z, t) \times \left(1 + \frac{1}{I_s}\{I(\mathbf{r}, z, t) + I(\mathbf{r}, 2L - z, t) + c\varepsilon b\,\mathrm{Re}[\tilde{E}(\mathbf{r}, z, t)\,\tilde{E}^*(\mathbf{r}, 2L - z, t)]\}\right), \tag{26}$$

where τ is the inversion population lifetime, consisting of a radiative and a non-radiative part

$$\tau^{-1} = \tau_r^{-1} + \tau_{nr}^{-1}, \tag{27}$$

I_s is the saturation intensity, $g_0(\mathbf{r}, z, t)$ is the small-signal gain, $I(\mathbf{r}, z, t)$ and $I(\mathbf{r}, 2L - z, t)$ are the field intensities, corresponding to the forward and backward modes respectively, and the superscript $(*)$ stands for the complex conjugate. The variable $b = 1$ accounts for mutual interference of the forward and backward waves i.e. transverse hole burning; an important effect in stationary media [21]. Atom movement due to diffusion, thermal motion, or gas flow, would partially wash out population modulation to a degree dependent on the flow velocity [4]; this may be accounted for by selecting a value of b between zero and unity. If atoms move more than one-half wavelength during the time the field is reflected back from a mirror, spatial-hole-burning effects are ignorable and $b = 0$.

Notice that the formulation is quite general and, unlike most analytic approximations, does not assume that the lasing medium uniformly fills the entire cavity; the dependence of the small-signal gain and power gain on the transverse and longitudinal coordinates may accurately model an arbitrary configuration.

3.2. Small-signal gain and saturation intensity

The small-signal gain g_0 is commonly assumed to be constant through the active medium and is usually determined experimentally by passing a probe CO_2 laser beam through the active medium. Alternatively, both the small-signal gain and saturation intensity I_s can be estimated by analysing the performance of the active medium as a laser [23]. These two parameters are critical in evaluating the discharge as a laser medium since their product $(g_0 I_s)$ represents the maximum available optical power density [24]. However, for laser design purposes there are many reported measurement techniques and results of these parameters under several operation circumstances [22, 23, 25–37] and some analytic approximations have been derived by solving analytically the simplified rate equations, providing models that agree reasonably well with the experimentally measured values in slow-flow diffusion-cooled CO_2 lasers and stationary gain medium [38].

For the particular case of transverse flow cw CO_2 laser systems, the rate equations have been solved analytically by Nath and Biswas [23], including the effects of gas flow and collisional transfer of energy between N_2 and CO_2 molecules and judiciously neglecting those processes whose effects are not too large for the sake of simplicity. The obtained expressions are of crucial importance since they explicitly depict the dependence of small-signal gain and saturation intensity on physical design parameters, such as on partial pressures of CO_2 and N_2, gas-flow velocity and pump rate. Although CO_2 gas dissociation is neglected in this model, since a gas residence time much shorter than 0.1 s is assumed [34], this effect may be accounted for by a suitable modification of the value of the ground level population density of CO_2. Further simplifications may be applied to the model to particularly slow or fast gas flow systems. Additionally, a self consistent quantum electrodynamic model to estimate the small-signal gain and other laser operation parameters was recently developed by Chang and Fluhler [39]; this model presents more accurate results than the conventional classic theory.

The assumption that the small-signal gain is constant through the lasing medium is reasonable when the tube diameter is much larger than the oscillation eigenstate radii; however, if this is not the case, the radial dependence of g_0 may significantly alter the mode competition, steady state output power and transverse intensity profile. It was found by Witteman [40] that in a sealed CO_2 laser, operating at peak power, a spatial mode switching is observed upon increasing the current. This effect has been attributed to a modification in the radial profile of the small-signal gain due to large discharge current [41, 42]. Thus radial variation of g_0 may significantly affect the modal competition and temporal and spatial cavity build-up on certain design parameters.

At very low discharge currents in wall dominated lasers, heating of the gas is minimal, and small-signal gain exhibits a zeroth-order Bessel function radial variation, thus reflecting the importance of the electron density profile in determining the upper level population [43]. However, upon increasing the current, the influence of gas temperature on the lower-level population is noticed. Approximately at 30 mA the increase in upper level population due to raising of the axial electron density is limited by the detrimental effect of the raising axial temperature. This saturating effect results in a quasi-constant distribution of the small-signal gain with certain independence

of the transverse radial coordinate everywhere except near the wall. When this situation occurs and the tube diameter is significantly larger than the mode radii, the small-signal gain may be considered to be constant.

If the current is further increased above approximately 50 mA, the axial small-signal gain is actually diminished and is less than at some points closer to the tube wall. This temperature effect on the CO_2 ground level is so strong that the magnitude of the axial gain is found to continuously decline with increasing current. The observed 'doughnut' gain radial profile explains the spatial mode switching that was reported by Witteman [40], since the lowest-loss cavity mode usually tends to concentrate its energy around the laser axis, an eigenmode with slightly higher diffraction losses and a 'doughnut' structure may have higher net cavity gain under this atypical gain profile [41, 42].

A similar small-signal gain profile behaviour was reported from previous measurements and computations for different gas mixtures, discharge pressures and CO_2 dissociation for wall dominated laser systems [41–43]. Although gain might be expected to increase with increasing current due to faster upper-level pumping, the strong influence of the gas temperature elevation leads to the opposite result. Thus rapid convective heat removal is critical to achieve high-power CO_2 laser devices.

Further physical resemblance may be achieved with the inclusion of a realistic radial dependence of the small-signal gain in the DCM method.

3.3. Inhomogeneous line broadening

Equation (26) is exclusive of homogeneous line broadening laser media, that occurs for instance in high-pressure gas lasers in which collisions between atoms or molecules become frequent enough so that lifetime termination and phase interruption dominate the broadening mechanism [22]. Inhomogeneous line broadening, however, occurs when the Doppler broadened linewidth is much wider than the natural linewidth, and the collision frequency is small compared to the spontaneous decay rates of the excited states, typical in very low-pressure gas discharge laser systems. It is well known that saturation of the inhomogeneous line takes place at a slower rate. Inspired on the non-dynamical commonly used relations for homogeneous and inhomogeneous line broadening laser media [22], we introduced a straightforward modification of the power gain dynamic equation (26) to account for inhomogeneous line broadening, namely

$$\tau \frac{\partial g(\mathbf{r},z,t)}{\partial t} = g_0(\mathbf{r},z,t) - g(\mathbf{r},z,t) \times \left(1 + \frac{1}{I_s}\{I(\mathbf{r},z,t) + I(\mathbf{r},2L-z,t) + c\varepsilon b\,\mathrm{Re}[\tilde{E}(\mathbf{r},z,t)\,\tilde{E}^*(\mathbf{r},2L-z,t)]\}\right)^{1/2}. \quad (28)$$

The inclusion of the dynamic gain equation leads to a complete set of equations for the DCM model, including expressions (A.6) and (A.7).

4. Numerical implementation

In order to test the proposed formulation, and compare it with other numerical methods and analytical approximations, we use it to retrieve laser turn-on dynamics. Although arbitrary spatio-temporal pump dependence can be represented with this method, the initial laser transitory with constant pump is widely studied and provides a perfect benchmark to check for the method accuracy.

The cavity equations of motion (A.6) and (A.7), including the dynamic gain (26), have been solved numerically for a typical resonator configuration. A positive branch circular confocal unstable resonator, operating on the 10.6 μm regime, was modelled using the previously described methodology; resonator length and magnification are $L = 3.24$ m and $M = 1.44$ respectively.

The output coupler is a graded reflectivity mirror with a radially varying power reflectivity profile given by

$$|\rho(r)|^2 = R_0 \exp[-2(r/a)^{14}], \quad (29)$$

where r is the transverse radial coordinate. Smoothing the output-mirror reflectivity profile in unstable resonators substantially reduces the intensity of the waves diffracted from the mirror edge, reducing computational requirements to properly model resonator modes and improving brightness and far-field intensity. In particular, super-Gaussian mirrors, as proposed and tested in unstable cavities by De Silvestri *et al* [44], have been found to combine the advantages of both hard-edge and Gaussian shapes: reflectivity smoothing avoids build-up of pronounced diffraction rings while the central almost constant reflectivity allows for wide filling of the active medium. The implemented output coupler peak reflectivity is $R_0 = 0.49$ and the mirror's spot size $a = 1.7$ cm.

Since the small-signal gain is assumed to be purely radially symmetric, coupling between different azimuthal symmetry modes is inhibited, as shown in equation (A.7), and proper gain saturation is only feasible by $l = 0$ symmetry modes; thus only the zeroth-order azimuthal symmetry modes are coupled by the numerical method.

To further reduce the computational effort, the coupling between different longitudinal modes was ignored by setting $q = q' = 0$ in equations (A.6) and (A.7); this is equivalent to assuming a single-frequency or highly monochromatic output beam.

The first step in solving the exact cavity equations is to numerically compute the bare cavity eigenmodes at the output mirror and everywhere inside the cavity where the gain is non-zero. For the present problem, the bare cavity modes just incident on the output mirror $u_{lp}(r, z = 2L^-)$ were computed by discretizing the integral (A.2) using the Gauss–Legendre quadrature scheme and diagonalizing the resulting matrix using standard numerical techniques. The adjoint eigenmodes at the reference plane are related to the forward modes by [4]

$$u^{\dagger}_{lp}(r, z = 2L^-) = u_{lp}(r, z = 2L^-)\,\rho(r) \times \exp\left[\frac{\mathrm{i}\pi}{\lambda B}(A - D)\,r^2\right]; \quad (30)$$

note that although $u_{lp}(r, z = 2L^-)$ is the forward propagating mode just incident on the output coupler, the adjoint mode

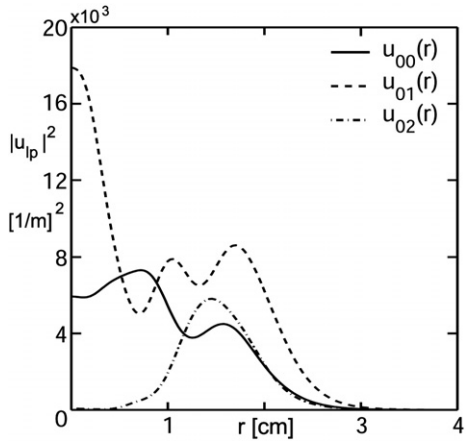

Figure 2. Transverse intensity distribution incident on the output mirror of the first three lowest-loss $l = 0$ bare cavity eigenmodes.

$u^{\dagger}_{lp}(r, z = 2L^{-})$ is propagating backwards and is just leaving the reference plane. Power gain is discretized in 40 gain sheets evenly distributed over the active medium along the axial coordinate from $z = 2.1$ to 3 m. The forward and adjoint modes are computed at the axial position of each gain sheet, propagating the mode from the reference plane by numerically solving the Huygens integral using the same Gauss–Legendre quadrature, and normalizing according to expression (A.5). How well the biorthogonality is satisfied numerically is a good check on the accuracy of the computed modes.

Transverse modes computed on the surface of the output mirror satisfy equation (A.5) within a 10^{-11} tolerance, while the modes inside the cavity satisfy it to better than one part in a thousand. All codes were written in Matlab software, mainly because of the existence of a wealth of built-in mathematical functions. Figure 2 depicts the computed field intensity distribution incident on the output coupler of the first three lowest-loss bare cavity transverse modes with $l = 0$ azimuthal symmetry. Mode indices are assigned according to their diffractive losses.

Homogeneous line broadening power gain, typical in high pressure CO_2 lasers, is assumed. Radial variation of the small-signal gain is accounted for with the generic function

$$g_0(r) = g_0\left(1 - c_1 r^2 + c_2 r^4 - c_3 r^6\right), \qquad r \leqslant R. \quad (31)$$

Here $g_0 = 0.01$ cm^{-1} is the longitudinally averaged axial small-signal gain coefficient, and the empirically determined coefficients that shape the gain profile are [4]

$$c_1 = 1.5606 \times 10^2 \text{ m}^{-2}, \quad (32)$$

$$c_2 = 8.664 \times 10^4 \text{ m}^{-4}, \quad (33)$$

$$c_3 = 2.249 \times 10^7 \text{ m}^{-6}. \quad (34)$$

This particular distribution, shown in figure 3, accounts for the radial decrease in gain due to collisional deactivation with the cylindrical gain tube wall of radius $R = 5.1$ cm and is consistent with experimental and theoretical bell shaped gain profiles reported for low discharge current in CO_2 amplifiers [41]. Transverse hole burning effects are neglected by setting $b = 0$ in equation (26), assuming sufficiently

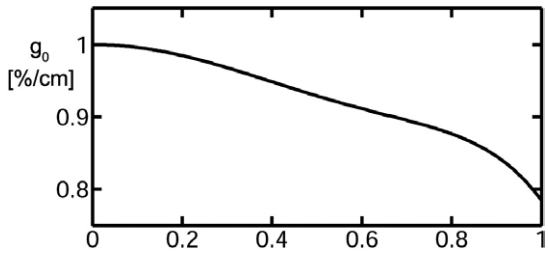

Figure 3. Radial variation of the implemented small-signal gain; the radial coordinate is normalized to the tube radius.

large axial gas flow. Average saturation intensity reported for this particular tube is $I_s = 3.404$ W cm^{-2} and implemented inversion population lifetime [45] is $\tau = 20$ μs.

The gain region was radially sampled using a Gauss–Legendre quadrature in order to compute the integral over the radial coordinate appearing in (A.7); the integrand over the axial coordinate was found to change very smoothly, thus a simple trapezoidal rule was found to be sufficient. Temporal integration of modal coefficients (A.6), (A.7), and dynamic gain equation (26), was computed using an adaptive step fourth-order Runge–Kutta algorithm.

The power gain initial condition is set to zero, $g(\mathbf{r}, z, t) = 0$, to allow a complete gain build-up from the small-signal gain, which is strongly related to the population inversion density, thus allowing retrieval of realistic temporal behaviour of laser start-up dynamics.

Numerical determination of the initial conditions for the expansion coefficients $A_{0p0}(t)$ is not a trivial problem; the initial field profile within the cavity should be primarily determined by spontaneous emission and is related to the small-signal gain distribution. A particular field profile may be inserted as the electric field initial condition by an appropriate expansion into the biorthogonal functions $u_{lp}(r, z)$; although one might be tempted to obtain these expansion coefficients by solving quadrature integrals with the adjoint set of functions, it has been shown that superior results are obtained by means of a procedure based on inverting the eigenmode orthogonality matrix [46].

Nevertheless, we have found that the steady state solution and mode temporal evolution are quite insensitive to the modal amplitude coefficients initial conditions provided they are non-zero and small compared to their steady state value; the modal amplitudes, whose initial values were chosen rather arbitrarily, rapidly decay in an exponential manner to a very small value that can effectively be sustained by the lasing medium, thus beginning the power gain saturation process. The damping rate coefficient of this decay process depends, of course, on modal diffraction losses and is different for each modal amplitude. To numerically check the validity of this assumption, we initially set each modal amplitude $A_{0p0}(t = 0)$ to the same initial value and compare the results to different random complex initial values; we find that the overall lasing dynamics remains practically unchanged as expected.

To ensure proper field modelling, it is crucial to check the convergence of the DCM method with respect to the number of transverse eigenmodes used in the electric field expansion. Figure 4 shows the steady state (a) intracavity

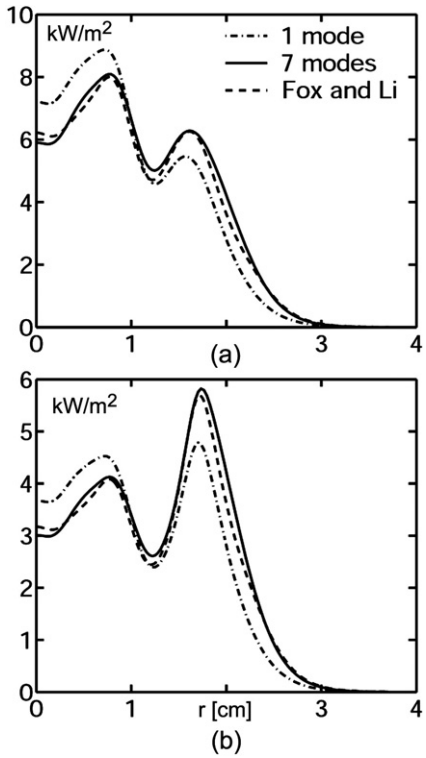

Figure 4. Steady state gain loaded (a) intracavity (incident on the output coupler) and (b) output intensity distribution. Results from the DCM method using one and seven transverse modes in the basis set are compared to those obtained from the iterative Fox and Li approach.

intensity distribution just incident on the output mirror and (b) output intensity distribution for a different number of transverse modes. We found that seven modes are sufficient to properly describe the loaded cavity field in this particular resonator.

The complete time dependence of the absolute value of the modal amplitudes, neglecting transverse hole burning, with the first seven lowest-loss $l = 0$ transverse modes coupled is shown in figure 5. The expansion coefficients were found to reach a steady state value after 300 μs. During the first 30 μs gain building occurs with negligible emission; the first spike appears soon after power gain passes its steady state value and the laser net gain then exceeds diffractive losses.

Temporal evolution of output power without transverse hole burning is depicted in figure 6(a). For comparison purposes, the numerical model was also implemented including mutual interference effects of the forward and backward wave on gain saturation by setting $b = 1$ in (26), thus accounting for stationary lasing media. Similar convergence checks were performed to ensure that enough modes were used in the expansion. A reduction of 15% of the output power was observed, as expected. The inclusion of coherent saturation reduces energy extraction and laser output power [4]; these results confirm the importance of fast gas flow to achieve high output power in CO_2 laser systems.

Spiking and damped-oscillating behaviour of output power can be observed in figure 6(a). The discrete, sharp, large-amplitude pulses appearing upon initial turn-on and their evolution towards the well documented small-amplitude, quasi-sinusoidal, exponentially damped relaxation oscillations [45] have been reported for laser systems in which the recovery time of the excited state population inversion is substantially longer than the laser cavity decay time [16].

Although this behaviour is not generally observed in most gas lasers, unstable resonators tend to have very short cavity decay times. Cavity lifetime or exponential cavity decay time is given by $\tau_c = T/\delta_c$; where $T \simeq 21.6$ ns is the approximate round-trip time of this resonator and $\delta_c \simeq 70\%$ is the round-trip cavity losses computed from the lowest-loss modal eigenvalue. The approximate value of the cavity decay time is $\tau_c \simeq 30.5$ ns, which is substantially shorter than the implemented population inversion decay rate ($\tau = 20$ μs), thus accounting for laser spiking and pronounced relaxation oscillations. Note that the interval between the early, large-amplitude spikes slightly decreases from spike to spike, evolving asymptotically to the period of the damped quasi-sinusoidal behaviour toward which the laser system evolves. This particular behaviour, also observed in reported experimental measurements [12, 16], occurs because power gain does not drop all the way to zero following a spike, as shown in figure 6(b), hence each successive spike starts from initial conditions that come closer to the laser steady state.

A rough estimate of the relaxation oscillation frequency can be obtained by the expression $\omega_{sp} = \sqrt{(r-1)/(\tau_c \tau)} \simeq 1.08 \times 10^6$ rad s^{-1}, obtained by solving a linearized small-signal version of the single-mode, single-atomic-level rate equations [16] and assuming that the laser is pumped to 50% above threshold ($r = 1.5$). The relaxation oscillation frequency estimated from output power small oscillations computed with the DCM with dynamic gain, as shown in figure 6(a), is $\omega_{sp} \simeq 1.13 \times 10^6$ rad s^{-1}. This fairly good agreement further illustrates the reliability of the new formulation.

Solution of the DCM with a dynamic gain equation permits retrieval of gain build-up and saturation at every point of the lasing medium. Temporal plotting of local power gain (see figure 6(b)) depicts a power to gain relationship strongly resembling results of numerically solving the single-mode rate equations for cavity photon number and population inversion [16]. The observed correspondence of local gain depletion and output power spiking and relaxation oscillations strongly resembles previously reported measurements, and ensures that the numerical method is properly describing matter–light interaction and realistic lasing dynamics.

When implementing this particular example we immediately noticed the effects of small-signal gain radial dependence on laser modal competition. Eigenvalues of the second and third lowest-loss modes (γ_{01}, γ_{02}) are near degenerate, and have very close steady state modal coefficient values if a uniform small-signal gain is implemented. However, upon introducing gain radial variation, the difference of field profiles of this modes comes into play, thus decreasing degeneracy and separating their steady state modal coefficient values. This illustrates the efficacy of the formulation to model the dynamics of modal competition and discrimination under different pumping schemes.

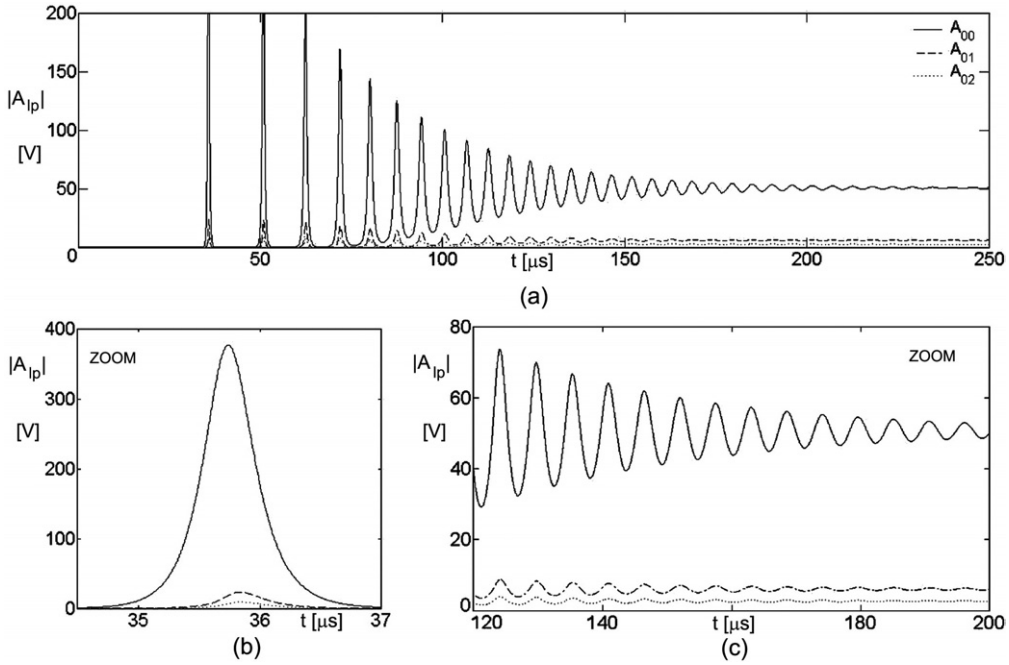

Figure 5. Temporal evolution of absolute value of the three lowest-loss modal amplitudes, using the seven lowest-loss $l = 0$ transverse modes in the basis set. (a) Full evolution to a steady state. (b) Zoom of modal competition in the first laser spike. (c) Zoom of modal competition in relaxation oscillations.

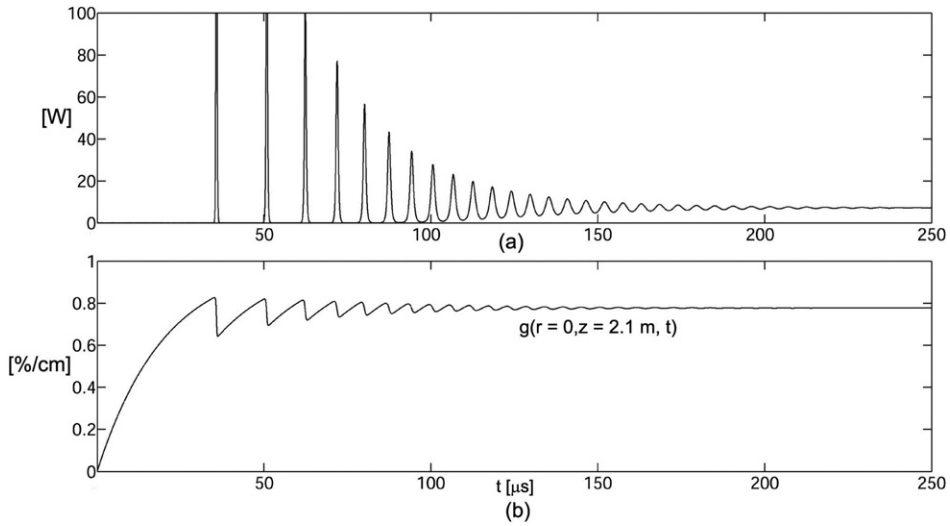

Figure 6. (a) Temporal evolution of computed laser output power without transverse hole burning. Behaviour depicts spiking and relaxation oscillations that evolve to a final steady state value. (b) Local gain $[g(r = 0, z = 2.1\ m, t)]$ build-up at a particular axial position; gain is partially depleted during the laser spike and evolves asymptotically to its steady state value.

4.1. Comparison with the Fox–Li method

The steady state field distribution obtained with the DCM method can be compared to the converged wavefront obtained from the Fox–Li iterative method as was previously implemented by Sziklas and Siegman [47]. The resonant cavity is divided into a number of axial segments; an arbitrary initial field profile is iteratively propagated from each segment to the next in free-space fashion using plane-wave beam decomposition and multiplied by the gain transverse distribution until it reaches a steady state. Taking advantage of axial symmetry, a previously reported discrete Hankel transform algorithm [48] is implemented to retrieve the field spatial frequency content. After each complete round trip of the circulating wave, the saturated gain profile across each segment is recalculated using the local wave intensity.

Because the Fox–Li method is restricted to the field steady-state solution, the dynamic gain equation as shown in equation (26) cannot be implemented. Upon neglecting gain temporal dependence we arrive at the conventional non-dynamic equation for homogeneously broadening medium as in expression (25), where transverse spatial hole burning is

neglected for direct comparison with results obtained from the numerical implementation of the DCM method.

Figure 4 shows the comparison between the intracavity and output intensity profiles retrieved with the Fox–Li method and those obtained from the steady state of the DCM method for different numbers of transverse modes in the basis set. Although there are some quantitative differences, it is evident that the distributions exhibit the same qualitative structure; note that upon increasing the number of lowest-loss modes that are included in the basis set, better agreement between the two different approaches is achieved.

5. Conclusions

This paper fully describes the DCM method, used to compute the time dependent three-dimensional loaded cavity field as an expansion in the bare cavity modes. Though it provided a solid method to analyse mode competition in unstable resonators, the use of the non-dynamic gain equation limited its use to steady state laser output. Upon the inclusion of the dynamic gain equation into this model, as proposed through this work, accurate retrieval of modal amplitude temporal evolution is possible. Inclusion of time dependent small-signal gain may account for discontinuous pumping and allows the analysis of transverse and longitudinal mode competition in gain-switched or pulsed lasers, and accurate modelling of spiking or stabilization transients.

The presented formulation will be particularly valuable to study pulsed lasers or those that do not reach a steady state output. We have successfully applied this formulation with a dynamic gain equation to accurately retrieve the well understood laser turn-on dynamics. Physical laser spiking and relaxation oscillations are obtained, as expected from cavity decay time and population inversion lifetime. Comparison of relaxation oscillation frequency retrieved with the proposed method and that estimated from a linearized small-signal analysis, that has been checked experimentally in a number of lasers [16], gave excellent results. Although we chose the implementation on laser turn-on with constant pump in order to meet the limitations of the algorithms we used for comparison purposes, the proposed formulation may model an arbitrary temporal variation of the laser pumping by a suitable modification of the small-signal gain, providing further insight of modal competition within unstable resonators.

Furthermore, the accurate modelling of pronounced laser spiking and relaxation oscillations, see figure 6(a), and power evolution resemblance to reported measurements for various lasing materials (such as Nd:YAG, ruby or organic dye lasers), confirm that the formulation can be extended to model solid-state or organic lasers [12, 13, 16].

The main advantage of using the DCM method with a dynamic gain equation is that it offers a rigorous and convenient approach to compute laser performance and stability. Giving a much more complete temporal and spatial description of the cavity field and lasing medium than the conventional Fox and Li approach, which is limited to compute the steady state field distribution.

The inclusion of a dynamic gain equation and gain radial profiles into the dynamic coupled mode method combined with the numerous reported experimental values and theoretical approximations to obtain realistic laser physical parameters, provide a valuable tool for design and prediction of beam spatial features, lasing transient and stability characteristics.

Acknowledgments

This research was partially supported by Consejo Nacional de Ciencia y Tecnología of México under grant 42808, and by the Tecnológico de Monterrey Research Chair in Optics under grant CAT–007.

Appendix. Axial symmetry considerations in the dynamic coupled mode method

For completeness and to establish useful notation we will briefly describe the simplifications to the DCM method regarding axial symmetry considerations. The equations that are derived in this section are cited in previous sections.

The derivation of the DCM method that is included in section 2 holds for any symmetry on the output coupler, assuming only that the paraxial system is symmetric. Although a more general expression of the propagation integral may be applied [4] the vast majority of laser resonators have symmetric paraxial systems. Nevertheless most of the optical cavities have circular primary and output mirrors, hence it is useful to apply further simplifications to the model regarding the axial symmetry.

The transverse eigenmodes may be decomposed into azimuthal components,

$$u_{lp}(\mathbf{r}, z) = u_{lp}(r, z)\exp(\mathrm{i}l\theta), \tag{A.1}$$

where l and p denote the azimuthal and radial mode index respectively. Assuming that the output coupler reflectivity and phase are exclusively radially dependent, each component is found to satisfy

$$\gamma_{lp}u_{lp}\left(r, z = 2L^{-}\right) = \frac{k_0\mathrm{i}^{l+1}}{B}\int r'\rho\left(r'\right)u_{lp}\left(r', z = 2L^{-}\right) \times J_l\left(\frac{k_0 r r'}{B}\right)\exp\left[-\frac{\mathrm{i}k_0}{2B}\left(Ar'^2 + Dr^2\right)\right]\mathrm{d}r', \tag{A.2}$$

where J_l is the lth order Bessel function of the first kind. Note that the eigenmode problem became a single integral, thus allowing a numerical representation as a matrix operator and the use of well known diagonalization algorithms.

The complex phasor amplitude is expanded as follows:

$$\tilde{E}(\mathbf{r}, z, t) = \sum_{l=-\infty}^{\infty}\sum_{p=0}^{\infty}A_{lp}(z, t)\,E_{lp}(\mathbf{r}, z), \tag{A.3}$$

$$E_{lp}(\mathbf{r}, z) = u_{lp}(\mathbf{r}, z)\exp[(\alpha_{lp} - \mathrm{i}\beta_{lp})(z - 2L)/c], \tag{A.4}$$

and the biorthogonality relationship now reads

$$\int_0^{\infty} r\,\mathrm{d}r\int_0^{2\pi}u_{lp}(r, z)\,u^{\dagger}_{l'p'}(r, z) \times \exp[\mathrm{i}(l - l')\theta]\,\mathrm{d}\theta = \delta_{ll'}\delta_{pp'}. \tag{A.5}$$

Expanding the amplitude coefficients $A_{lp}(z, t)$ in a Fourier series of longitudinal modes, and using (A.5), the

resultant equation of motion for the exclusively time dependent coefficients is

$$\frac{\mathrm{d}A_{lpq}}{\mathrm{d}t} + \left[(\alpha_0 + \alpha_{lp}) - \mathrm{i}\left(\beta_{lp} + \frac{\pi q c}{L}\right)\right] A_{lpq}\,(t) = \frac{c}{4L}\sum_{lpq} \mathbf{G}_{lpq,l'p'q'}\,(t)\,A_{l'p'q'}\,(t)\,, \tag{A.6}$$

with

$$\begin{aligned}\mathbf{G}_{lpq,l'p'q'}\,(t) = {} & \int_0^{2L} \mathrm{d}z \exp[\mathrm{i}\pi z(q-q')/L] \\ & \times \exp\{[(\alpha_{l'p'} - \alpha_{lp}) - \mathrm{i}(\beta_{l'p'} - \beta_{lp})](z-2L)/c\} \\ & \times \int_0^{2\pi} \mathrm{d}\theta \exp(\mathrm{i}[l'-l]\theta) \\ & \times \int_0^{\infty} \mathrm{d}r\, r u^{\dagger}_{lp}(r,z) g(\mathbf{r},z,t) u_{l'p'}(r,z).\end{aligned} \tag{A.7}$$

In equations (A.6) and (A.7) the coupling of radial, azimuthal and longitudinal modes can be observed.

References

[1] Fox A G and Li T 1963 *Proc. IEEE* **51** 80
[2] Fox A G and Li T 1961 *Bell Syst. Tech. J.* **40** 453
[3] Siegman A E 1980 *Appl. Phys. Lett.* **36** 412
[4] Oughstun K E 1987 *Unstable Resonator Modes in Progress in Optics* vol 24, ed E Wolf (Amsterdam: North-Holland)
[5] Bowers M S and Moody S E 1990 *Appl. Opt.* **29** 3905
[6] Siegman A E 1965 *Proc. IEEE* **53** 277
[7] Bowers M S and Moody S E 1994 *J. Opt. Soc. Am.* B **11** 2266
[8] Lugiato L A, Prati F, Narducci L M, Ru P, Tredicce J R and Bandy D K 1988 *Phys. Rev.* A **37** 3847
[9] Rahman L and Winful H G 1993 *Opt. Lett.* **18** 128
[10] Casperson L W 1976 *J. Appl. Phys.* **47** 4555
[11] Mossakowska-Wyszynska A, Witonski P and Szczepanski P 2002 *Appl. Opt.* **41** 1668
[12] Lin C 1975 *IEEE J. Quantum Electron.* **11** 602
[13] Menne T J 1966 *IEEE J. Quantum Electron.* **2** 38
[14] Siegman A E 1979 *Opt. Commun.* **31** 369
[15] Wright E M and Firth W J 1982 *Opt. Commun.* **40** 410
[16] Siegman A E 1986 *Lasers* (California: University Science Books)
[17] Oughstun K E 1982 *Opt. Commun.* **42** 72
[18] Parent A, McCarthy N and Lavigne P 1987 *IEEE J. Quantum Electron.* **23** 222
[19] Ferguson T R 1992 *Appl. Opt.* **31** 7551
[20] Fox A G and Li T 1966 *IEEE J. Quantum Electron.* **2** 774
[21] Lax M, Agrawal G P, Belic M, Coffey B J and Louisell W H 1985 *J. Opt. Soc. Am.* A **2** 731
[22] Freed L E, Freed C and O'Donnell R G 1982 *IEEE J. Quantum Electron.* **18** 1229
[23] Nath A K and Biswas A K 1997 *IEEE J. Quantum Electron.* **33** 1278
[24] Fowler M C 1971 *Appl. Phys. Lett.* **18** 175
[25] Deutsch T F 1967 *IEEE J. Quantum Electron.* **3** 151
[26] Antropov E T, Silin-Bekchurin I A, Sobolev N N and Sokovikov V V 1968 *IEEE J. Quantum Electron.* **4** 790
[27] Cheo P K 1967 *IEEE J. Quantum Electron.* **3** 683
[28] Bletzinger P, LaBorde D A, Bailey W F, Long W H Jr, Tannen P D and Garscadden A 1975 *IEEE J. Quantum Electron.* **11** 317
[29] Patel B S 1973 *IEEE J. Quantum Electron.* **9** 1150
[30] Edighoffer J A, Boehmer H, Caponi M Z, Fornaca S, Munch J, Neil G R, Saur B and Shih C 1983 *IEEE J. Quantum Electron.* **19** 316
[31] Degnan J J, Walker H E, McElroy J H and McAvoy N 1973 *IEEE J. Quantum Electron.* **9** 489
[32] Djeu N, Kan T and Wolga G J 1968 *IEEE J. Quantum Electron.* **4** 256
[33] DesAutels G L, Daniels D, Bagford J O and Lander M 2003 *J. Opt. A: Pure Appl. Opt.* **5** 96
[34] Siemsen K J, Reid J and Dang C 1980 *IEEE J. Quantum Electron.* **16** 668
[35] Takahashi N, Saski T and Gamo H 1991 *Appl. Opt.* **30** 3805
[36] Kroeker D F, DeFaccio M A, Pindroh A L, Guyer D R, Fisher C H and Moody S E 1989 *Appl. Opt.* **5** 897
[37] Smith D C 1971 *IEEE J. Quantum Electron.* **7** 459
[38] Lax M, Louisell W H and McKnight W B 1975 *Phys. Rev.* A **11** 1365
[39] Chang C S and Fluhler H U 1990 *J. Opt. Soc. Am.* B **7** 2061
[40] Witteman W J 1968 *IEEE J. Quantum Electron.* **4** 786
[41] Franzen D L and Collins R J 1972 *IEEE J. Quantum Electron.* **8** 400
[42] Franzen D L and Collins R K 1972 *IEEE J. Quantum Electron.* **8** 758
[43] Wiegand W J, Fowler M C and Benda J A 1971 *Appl. Phys. Lett.* **18** 365
[44] De Silvestri S, Laporta P, Magni V, Svelto O and Majocchi B 1988 *Opt. Lett.* **13** 201
[45] Svelto O 1998 *Principles of Lasers* 4th edn (New York: Plenum)
[46] Kostenbauder A, Sun Y and Siegman A E 1997 *J. Opt. Soc. Am.* A **14** 1780
[47] Sziklas E A and Siegman A E 1975 *Appl. Opt.* **14** 1874
[48] Guizar-Sicairos M and Gutiérrez-Vega J C 2004 *J. Opt. Soc. Am.* A **21** 53